



Subsurface Dynamic Deformation and Nano-structural Evolution in 40Cr Steel Under Dry Sliding Wear

Shuang Liang¹ · Peng Zhu¹ · Yudan Yang¹ · Xing He¹ · Wurong Wang¹ · Xicheng Wei¹

Received: 23 November 2018 / Accepted: 8 August 2019 / Published online: 20 August 2019
© Springer Science+Business Media, LLC, part of Springer Nature 2019

Abstract

Dry sliding tribological properties of normalized 40Cr steel pins against quenched and tempered GCr15 discs were investigated under various sliding distances through disc-on-pin contact configuration. Microstructural feature evolution and strain-hardening behavior of worn subsurface in 40Cr pins were systematically analyzed using scanning electron microscopy and transmission electron microscopy. It is found that based on the variation of wear rate, three stages can be divided throughout the friction process: initial wear, slow wear and stable wear. The corresponding microstructures beneath contact surface are subjected to significant strain-hardening effect and structural rearrangement. Nano-grains of 40–100 nm are produced in the topmost subsurface layer and the nanocrystallization mechanism during friction process is further elucidated. Pronounced vortex structures are generated in the localized subsurface zones due to high strain localization and shear instability. With the prolongation of sliding distances, vortex structures suffer dynamic embrittlement and exfoliation from the wear surface as a result of periodically excessive hardening effect, leading to the high wear rate in stable wear stage.

Keywords 40Cr steel · Tribolayer · Vortex structure · Nanocrystallization mechanism

1 Introduction

It has been well recognized that the sliding contact between materials can induce large plastic deformation and strain gradient underneath the worn surface, the corresponding subsurface structures will accordingly suffer drastic changes and may induce severely deformed or even newly formed layer structures [1, 2], which are generally called as the “tribofilm” or “tribolayer”. Occurrence of such structures will doubtlessly influence the wear mechanism of materials [3–5]. Great efforts have been made on the investigations of subsurface microstructural evolution during friction contact. Rigney’s [6] experimental results show that the plastic deformation, interaction with environment, mechanical mixing and flow patterns produced by friction were the main features during the evolution of tribomaterials. Yao et al. [7] have also concluded that the transformation from the subsurface dynamic recrystallization structure (DRX) into the top nanostructured mixing layer (NML) was the most important

process which could determine the wear mechanism of pure copper. Korres et al. [8] have been able to in situ observe how the surface deformation, material transfer and wear affected the topography while revealing a gradient structure from the nanocrystalline to ultrafine crystalline beneath Cu worn surface. Recently, available researches [9, 10] have reported the formation of ultra-refine or nanolaminated structures induced by subsurface deformation. On this basis, new techniques such as surface mechanical grinding treatment (SMGT) [11] have been developed and successfully applied to preparing a gradient nanograined surface layer on metals to improve their mechanical properties.

For all that, present investigations on the characteristics of tribofilm or ultrafine structures beneath worn surface are mainly concentrated in the ductile materials such as copper [12], nickel [11] and aluminum [13]. But for conventional structural steels with complicated multiphase, which are generally applied in the friction pair of mechanical transmission components. Although there is a vast body of literature on the friction and wear behavior of such materials, most of them are confined to the basic tribological properties and only few papers have reported the detailed evolution mechanism of friction-induced subsurface structures. A more complete understanding of the relationship between

✉ Xicheng Wei
wxc1028@shu.edu.cn

¹ School of Materials Science and Engineering, Shanghai University, Shanghai 200444, China

the subsurface evolution and its effect on the tribological failure of steels is still lacking. Therefore, it is quite necessary to implement further studies into the commonly used ferrite–pearlite steels to understand the subsurface deformation and evolution mechanism, which will not only help to further reveal the tribological essence, but also to improve the performance of conventional materials for practical engineering applications.

In this study, a series of dry sliding wear tests of normalized 40Cr pins with different sliding distances was carried out to investigate the wear behavior and subsurface changes under friction contact. Two points are emphasized in the article: one is to further understand the forming mechanism of nanolaminated structures in the near-surface region of ferrite–pearlite steels during friction process; the other is to discuss the vortex structure evolution underneath the worn surface and its possible influence on the wear properties of materials.

2 Experimental Details

2.1 Sample Preparation

Commercial 40Cr steel and GCr15 steel with chemical compositions tabulated in Table 1 were respectively employed as pin and disc materials. The 40Cr steel was EDM-wire-cut and machined into $\Phi 6$ mm \times 8 mm specimens after normalized at 850 °C, with a hardness of 222 HBW. The GCr15 discs were oil quenched at 830 °C and then tempered at 180 °C for 2 h after machined into the dimension of $\Phi 35$ mm \times 5 mm, achieving a hardness of 60 HRC.

2.2 Friction and Wear Tests

Unlubricated sliding wear tests were performed on a MMW-1 tribometer in disc-on-pin contact configuration as shown in Fig. 1. Prior to each test, both pin and the counterpart surfaces were slightly wet polished with SiC emery papers up to 1200 grit to achieve a final surface roughness (Ra) of 0.07 μ m and 0.04 μ m, respectively. The friction and wear tests were carried out at room temperature (298 K) with a normal load of 150 N, a gyration radius of 11 mm and a sliding speed of 0.46 m/s. Different sliding distances of 414–6624 m were individually selected to investigate the evolution of wear behavior and worn surface/subsurface changes. All tests with different sliding distances were

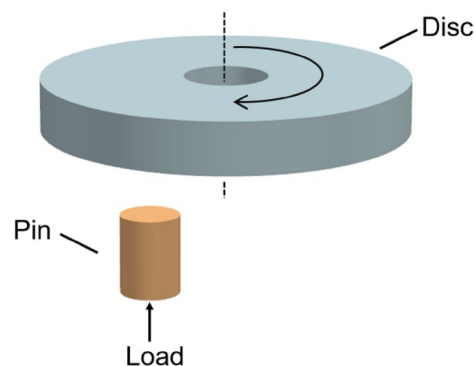


Fig. 1 Schematic diagram of disc-on-pin friction contact mode

respectively repeated for three times. Before and after each test, specimens were ultrasonically cleaned with a mixed solvent of acetone and ethanol for 10 min and then dried in 60 °C drying oven.

2.3 Microstructure Characterization

The mass loss of samples was measured through Praxium124-1CN precision electronic balance with 0.1 mg resolution and the wear rate was calculated by $W = \Delta E / S$, where ΔE refers to the wear weight loss (mg), S to the sliding distance (m). After worn surface observations, the pins were cross-sectioned perpendicular to the center of wear scar and parallel to the sliding direction, then inlaid using epoxy resin to prepare cross-sectional specimens. Before cross-sectioning, the pins were nickel electrodeposited to protect the worn surface features against damage and edging effect. The middle region of cross-sectioned specimens was selected as the testing area of subsurface observation and microhardness determination, which were prepared by grinding, mechanical polishing and electrolytic polishing. The sectional morphologies were observed on a JSM-6700F field-emission scanning electron microscopy (FE-SEM) with an oxford energy-dispersive X-ray spectrometer (EDS). Detailed microstructural features with different depths beneath the worn surface were characterized through JEM-2100F transmission electron microscope (TEM), the plane-view foils for TEM analysis were prepared with the method depicted in Ref. [14]. The microhardness measurements were carried out across the section from the top surface to matrix on a MH-3L Vickers hardness tester, with a load of 10 g and a loading time of 10 s. The transverse distance of two adjacent

Table 1 Chemical compositions of 40Cr and GCr15 steel (wt%)

Material	C	Cr	Mn	Si	Ni	S	P
40Cr	0.434	0.893	0.644	0.242	0.026	0.007	0.014
GCr15	1.010	1.479	0.315	0.218	0.022	0.008	0.021

microhardness indents was kept three times larger than the maximum diagonal to prevent interactions between consecutive measurements [15]. Each reported hardness value was the average of at least seven effective measured results.

3 Results

3.1 Tribological Performance

Figure 2 exhibits the friction coefficient and wear rate variations versus sliding distances of the normalized 40Cr pins. Initially, the value of friction coefficient was low but soon

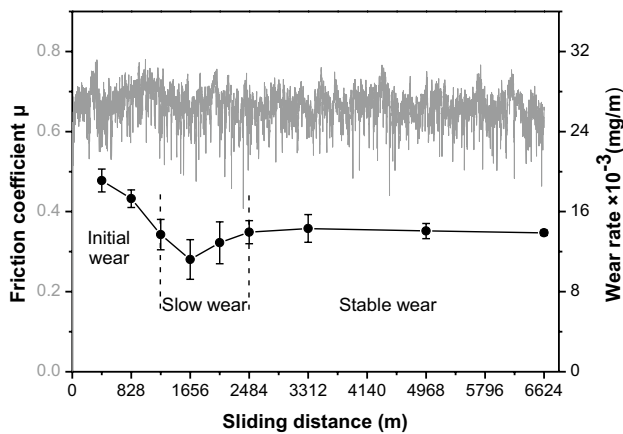


Fig. 2 Friction coefficient and wear rate variations of normalized 40Cr pins

increased to over 0.70 within 350 m sliding distance, then exhibiting no significant changes and remained stable at about 0.64 ± 0.05 as the sliding distances increased. Nevertheless, from the variation tendency of wear rate, the wear behavior of 40Cr samples could be divided into three typical stages: initial wear, slow wear and stable wear. At the initial wear stage, the wear rate of 40Cr pins was rather high and exhibited an obvious reduction trend. During the period between 1242 m and 2484 m, the wear rate decreased and then dramatically increased (reaching its minimum level when sliding for about 1656 m), which corresponds to the slow wear stage. Afterwards, with the prolongation of sliding distances, the wear rate tended to stabilize at $13.9 \pm 0.3 \times 10^{-3}$ mg/m, entering the stable wear stage.

The variation of wear rate indicates that the wear mechanism and corresponding subsurface microstructures of pin samples have undergone changes with the increase of sliding distances. Therefore, observations and analyses were conducted on the 40Cr pins with 414, 1656 and 6624 m sliding distance to study the surface/subsurface microstructure and property changes at different wear stages.

3.2 Worn Surface and Subsurface Microstructural Changes

Figure 3 shows the worn surface morphologies of normalized 40Cr pins and GCr15 counterparts with different sliding distances. Typical adhesive traces along the sliding direction and peeling off slices were the main surface characteristics of all pin samples while no abrasive particles could be detected on the worn surface, indicating that the main

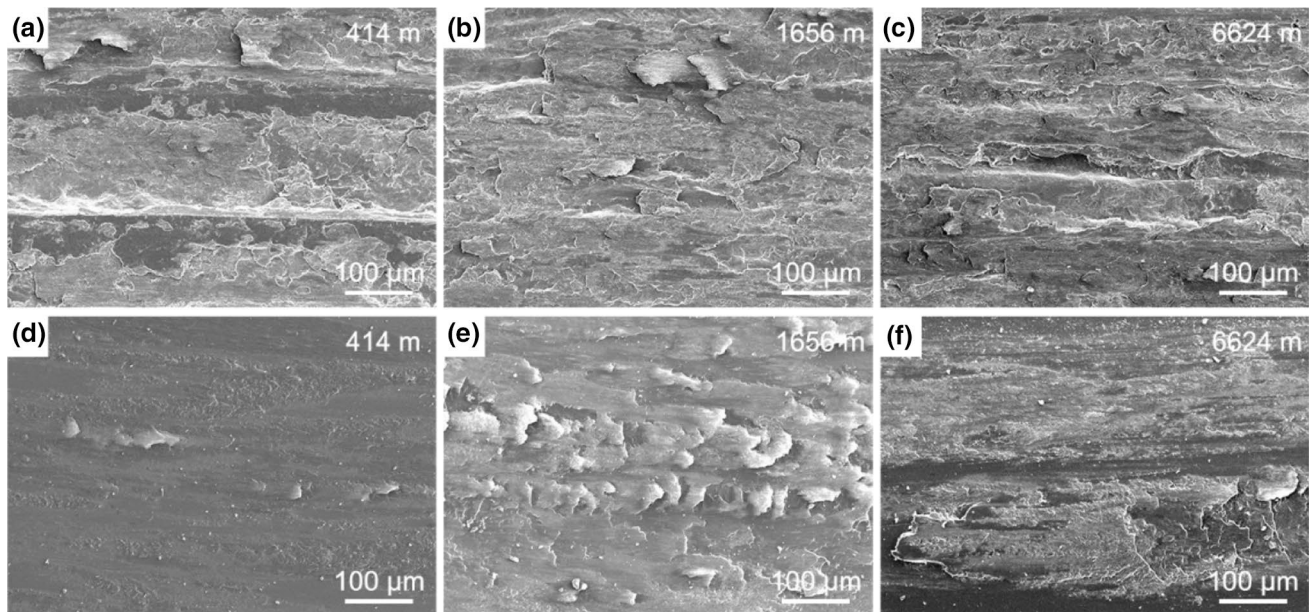


Fig. 3 Worn morphologies of the 40Cr pins (a–c) and GCr15 counterparts (d–f) with different sliding distances

wear mechanism in dry sliding was the severe adhesive wear accompanied with slight spalling. As a result of the adhesion effect, it is correspondingly illustrated from Fig. 3d–f that the squamous and bulgy materials have transferred from the pin to disc surfaces during friction process, which further accumulated into bulk adhesion with the increment of sliding distances.

Microstructures along the depth from worn surface into matrix were characterized through the cross-sectional SEM of normalized 40Cr pins, which were indicated in Fig. 4. Structurally, such distinct area could be divided into different zones as follows (the outer layer is protective Ni coating):

(II) The unpeeled delamination layer. In this layer, the observed pearlite and ferrite lamellar structures suffered obvious mechanical fracture and fragmentation, numerous cracks were found between the structure interfaces as a result of severe contact stresses and strains. The corresponding EDS analysis (Fig. 4d) proved the composition of this layer to be the same as matrix, indicating that there was no external deposition on the wear track of pin samples.

(I) The plastic deformation layer (PDL). In contrast to the matrix, a series of plastic flow lines were clearly observed in zone I, having a tendency to incline to the outmost sliding surface, similar to those reported in Ref. [16 and 17]. Such phenomenon suggests that the pearlite and ferrite structures beneath worn surface have suffered dramatic plastic deformation along sliding direction under the interaction of shear stress and friction heat. It also appears that closer to the worn surface resulted in severer deformation, corresponding to the laminar structures parallel to the upmost PDL. Detailed analyses were then carried out to distinguish

the microstructural differences in the PDL under different depths.

Figure 5 shows a bright-field (BF) TEM image with the depth span of 80–100 μm underneath the worn surface after sliding for 3312 m. In this section, the pearlite lamellar structures could be clearly identified, but the interlamellar spacing of pearlite structures suffered obvious diminishment, decreasing from nearly 200 nm to 90–150 nm. Low-density dislocation walls and dislocation lines (red arrows) were clearly observed in the lamellar structures.

Meanwhile, the outmost worn subsurface of pin samples after 3312 m sliding was characterized. Figure 6 shows the BF image with an inset of selected area electron diffraction (SAED) pattern and corresponding dark-field (DF) image of

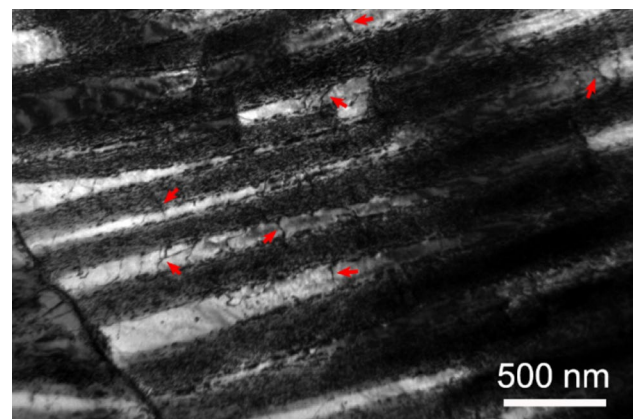


Fig. 5 TEM BF image of structures at depth of 80–100 μm beneath the worn surface of 40Cr pin after 3312 m sliding

Fig. 4 Cross-sectional microstructures of 40Cr pins after sliding for **a** 414 m, **b** 1656 m, and **c** 6624 m; **d** EDS spectrum of the squared region indicated in **c**

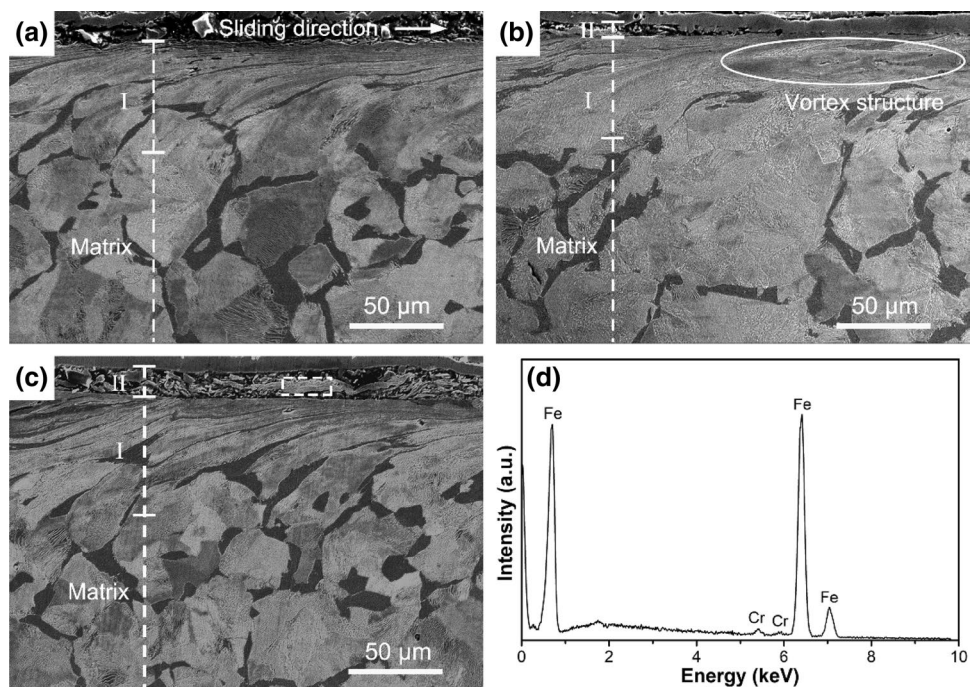
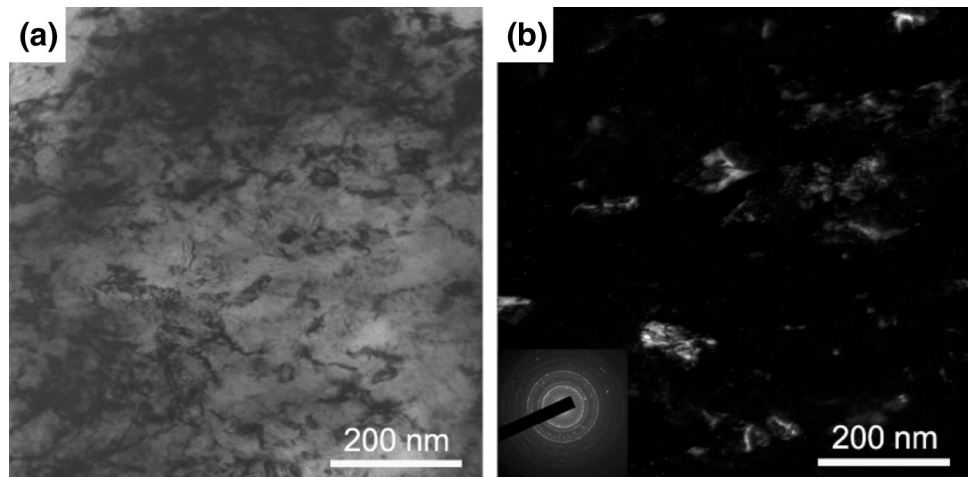


Fig. 6 TEM images of the outmost worn subsurface structures of 40Cr pin after 3312 m sliding: **a** BF image; **b** corresponding DF image with SAED pattern inserted



the outmost region. The original ferrite structures became homogeneous and the lamellar structures could not be identified, a great amount of dislocation cells appeared in the observed area. Uniform polycrystalline diffraction rings could be clearly observed in the SAED pattern, which means the ferrite grains and cementite particles in outmost subsurface possessed rather small sizes and random orientations. It is estimated from the DF image that the size of the grains in outmost worn subsurface was in the range of 40–100 nm.

It is well worth noting that differing from the normal plastic deformation zone, severely deformed turbulent flows (Fig. 4b) appeared continuously in some local zones of the upmost worn subsurface at the slow wear stage, which suffered the continuous accumulation along sliding direction and gradually developed into the vortex structures with complicated structural characteristics. Similar structures were possibly found in the near-surface region of alloys with low hardness and good plasticity [18, 19], but studies on the phenomenon about vortex structure and its effect on the tribological behavior of steels have been rarely reported.

3.3 Microhardness Gradient

Figure 7 illustrates the microhardness variations along the depth ranging from the worn surface to matrix after sliding for various distances. A gradually decreased microhardness distribution was found in the deformation layer with increasing depth beneath the worn surface, varied from more than 390 HV_{0.01} of the outmost layer to about 200 HV_{0.01} of the undeformed matrix. With the prolongation of sliding distances, microhardness of the upmost subsurface showed the trend which first increased and then decreased. Comparing the morphologies of upmost deformation zone with different sliding distances, it is worth noticing that the existence of vortex zone in outmost deformation layer with 1656 m sliding distance exhibited relatively high microhardness of 505 HV_{0.01}, which is similar to the results Yao et al. [20] found

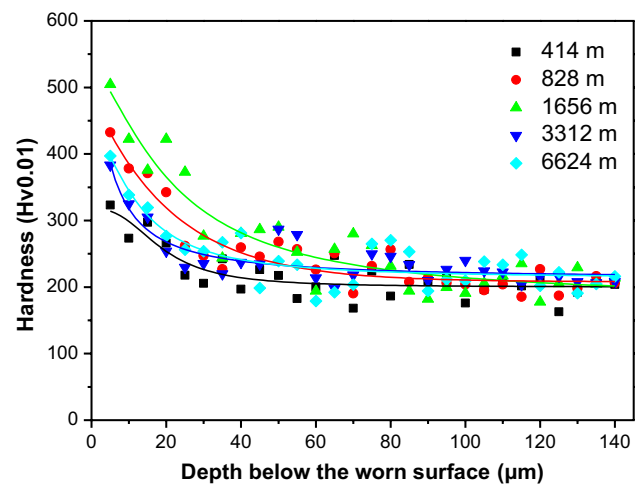


Fig. 7 Microhardness variations below the worn surface of 40Cr pins after different sliding distances

in pure copper. Causes for such phenomenon may lie in that the vortex structures are mainly composed of nanocrystalline induced by severe plastic deformation, resulting a hardening zone near the worn surface.

4 Discussion

4.1 Large Strain Distribution in PDL

During dry sliding friction, the tangential shear force induced by friction contact tends to plastically deform the near-surface materials. It has been reported that the friction process is usually accompanied with a large amount of cyclic plastic strains in rubbing contact [21], attributing to the formation of depth-dependent structure as shown in Fig. 4. The variations of shear strains along with depth from the worn surface were calculated using the curvature

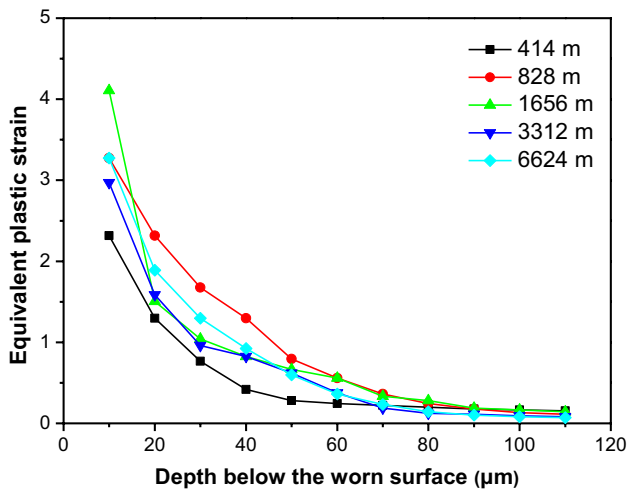


Fig. 8 Equivalent plastic strain variations below the worn surface of 40Cr pins after different sliding distances

of flow lines in the way described by Moore [1] and Venkataraman [22]. The equivalent strain $\varepsilon(Z)$ at depth Z beneath the worn surface can be calculated from the shear angle of the interface $\theta(Z)$, as the following equation:

$$\varepsilon(Z) = \frac{\sqrt{3}}{3} \tan[\theta(Z)]$$

Figure 8 presents the experimentally determined equivalent plastic strain distributions beneath the worn surface after sliding for 414–6624 m. The value of equivalent plastic strain gradually decreased with increased depth from the upmost worn subsurface until exceeding the undeformed matrix. Such phenomenon also reflects the degree of friction-induced plastic deformation below the wear surface. The plastic strain in subsurface could reach as high as 411% at the depth of 10 μm according to the curvature of flow line, corresponding to the high microhardness of 423 $\text{HV}_{0.01}$ at the same depth.

The shortcoming lies in that such an equation is not suitable for the equivalent strain estimation of parallel flow structures or vortex structures in severely deformed outmost layer. However, previous studies have shown that the shear strain at the topmost surface would be much higher than those in the subsurface. Sato et al. [23] have reported that the effective shear strain in the friction surface of Al–Al₃Ti could exceed the critical value of more than 52, as calculated based on the shear deformation for a spherical grain. Cai et al. [24] also claimed that the equivalent strain right below the sliding surface of eutectic Ag–Cu alloy could reach a maximum of 7.4, more than two times of that in the subsurface layer.

As is shown in Fig. 8, a comparatively high strain was clearly observed at depth of 10 μm with 1656 m sliding

distance, where the vortex structures formed in Fig. 4b. The main result of such a severe plastic deformation during friction process is the typical hardening effect and significant subsurface structural rearrangement, leading to the deformation misfit between refined sublayer and lower layers, creating intricately deformed structures [25]. It is believed that the high shear strain combined with flow localization will result in the generation of stress concentration, which may be responsible for the formation of vortex structures.

4.2 Mechanism of Subsurface Nanocrystallization

For a friction-induced deformation system, depth-dependent structures usually form owing to the strain gradient below worn surface [26]. In this part, in terms of detailed TEM investigations of the deformation subsurface with different depths under the worn surface, the forming mechanism of subsurface nanocrystallization is further discussed and concluded as following fundamental processes, as presented in Fig. 10.

Initially, the pearlite and ferrite structures undergo significant compressive stress which is perpendicular to the wear surface and the lamellar spacing obviously shrinks. Meanwhile, a large number of dislocations accumulate in the ferrite laths with plastic strain accumulation inside, which is shown in Fig. 5. It can also be observed that the dislocations take form and interact with each other in the cementite grains.

With the shear strains increasing, massive proportions of plate-like cementite grains suffer fragmentation and even dissolve afterwards (Fig. 9), transformed into rod-like particles. It is thought that the cementite thinning process and the formation of slip bands will increase the surface energy per volume and the instability of cementite, resulting in its dissolution [27]. At the same depth, the dislocation density

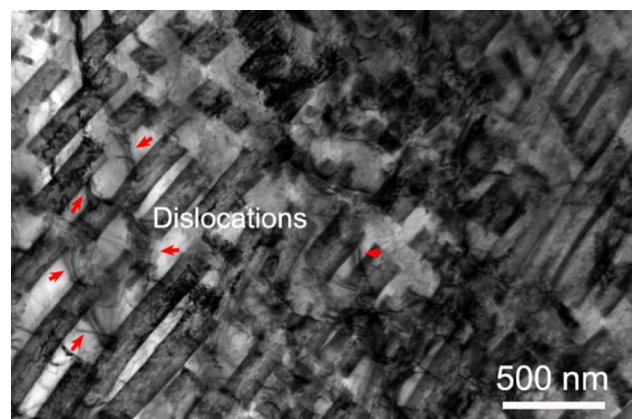


Fig. 9 TEM BF image of structures at depth of 50–70 μm below the worn surface of 40Cr pin after 3312 m sliding

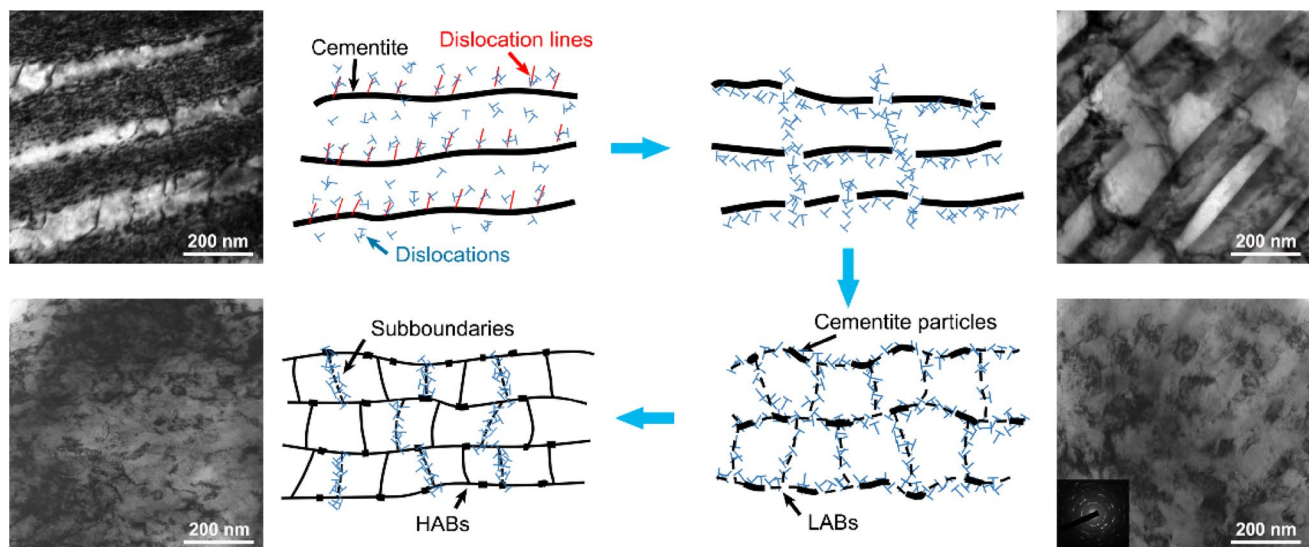


Fig. 10 Schematic diagram of the friction-induced surface nanocrystallization in ferrite–pearlite structures

in ferrite increases quickly due to strong plastic deformation. The moving, interacting and proliferating of dislocation tangles contribute to the diffusion and migration of carbon atoms from cementite boundaries to the distant ferrite structures, which is also the main driving factor for cementite dissolving. Zhang's analysis [28] showed apparent carbon concentration around 9–10 at % in the deformed cementite lamellar and 2–3 at % in the deformed ferrite, indicating the cementite fragmentation and decomposition under plastic deformation.

Within the depth span of 20–40 μm , the subsurface microstructures become relatively homogeneous. Original pearlite and ferrite lamellar structures could hardly be identified, approximately distributed in the form of microcrystalline grains. Such phenomenon can be explained as the increasing dislocation pinning effect vertical to dislocation walls with strain accumulation [29]. This behavior attributes to the transformation from dislocation walls into the subboundaries with small angle, dividing the original lamellar grains into more subgrains with smaller length to width ratio. The SAED pattern in Fig. 10 exhibits elongated spots and tends to form rings, indicating the comparatively small misorientations between these small-sized subgrains. It can be observed that almost all the cementite grains suffer dissolution and spheroidization, only a few fragmented yet undissolved cementite grains disperse around the refined ferrite boundaries in the shape of short bar or granule, which is analogous to the precipitation behavior of cementite particles under surface mechanical attrition treatment [30].

When the shear strain reaches a critical value, ultrafine or even nanocrystalline structures are usually formed below the worn surface. Closer to the outmost surface region, more dislocations are generated in the subboundaries,

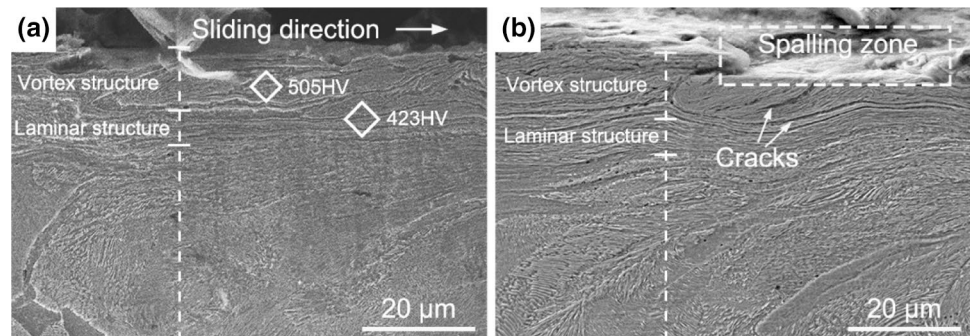
massive high-density dislocation walls and cells can be identified under dry friction, as showcased in Fig. 6. The slipping mechanism of deformation-induced dislocations in subboundaries will result in the grain rotation or the grain boundary sliding and accelerate the transformation from low-angle grain boundaries (LABs) into high-angle grain boundaries (HABs) [31]. The random orientations of nanocrystalline are assumed to result from the formation of HABs or the grain rotation under high strains. With strain accumulation, the subdivision takes place at a finer and finer scale. Such mechanism involves in the further grain refinement until the grain size reaches the stable minimum value [32].

4.3 Evolution Mechanism of Vortex Structures

It is well known that the continuous sliding friction will induce rather significant deformation which can easily refine the grain in subsurface layer. The so-called vortex structures have been reported in the subsurface of soft materials when the final stage of friction process is characterized by the generation of new deformation scale level (nanocrystalline layer) [20]. Tarasov [19] found that the vortex structure in pure copper is composed of smaller sublayers with mainly < 100 nm horizontally elongated grains, which may flow at different rates with each other.

As mentioned above, the possible reason for the formation of vortex structures is the strain localization occurring on the contact spots. Actually, when the high strain loaded, only some local contact spots (several percent of the nominal interacting surface) of materials exceed their yield strength and result in severe local deformation [33]. Therefore, during the late slow wear stage, stress of this sort together with

Fig. 11 Illustration for the near-surface vortex structure evolution with **a** 1656 m and **b** 6624 m sliding distance



the shear strain accumulation (1656 m in Fig. 8) probably contributes to the formation of permanent fragmented structures in subsurface layer, making the non-dislocation deformation of subsurface materials feasible. Such deformation can be either laminar or vertical [25], depending on the loading conditions and material characteristics. Then, the multi-scale substructure fragments are involved in both translation and rotary deformation, leading to the formation of vortex structure below worn surface. Generally, such translation-rotation structure is the result of strain localization and shear instability in dynamic deformation. Simulation results [34] also proved that the inhomogeneous deformation distribution and the heterogeneity of contact surface would lead to the generation and development of dynamic vortex structures in the tribolayer.

The surface strain-hardening effect during the early stage of sliding (< 1656 m) can suppress the formation of wear particles and thus will decrease the wear rate of pin samples, as indicated in Fig. 2. However, with the continuous strain accumulation, the hardening effect in near-surface reaches an ultimate level and thereby the vortex structures beneath worn surface will suffer plastic failure and embrittlement. Due to the property differences and the incompatibility between brittle vortex structures and surrounding laminar structures as Fig. 11 shows, microcracks initiate and tend to expand along the interface between such two structures with the prolongation of sliding process. Then, the vortex structures spall (Fig. 11b) and the laminar structures transform into vortex structures subsequently. These two processes go on repeatedly during the stage of stable wear. Such procedure is similar to the vortex evolution mechanism which Psakhie et al. put forward [34]: I. Uniform displacement bands forming; II. New vortex core nucleating; III. Growing and expelling process; IV. Size and velocity developing. The main result of such a periodic procedure lies in the formation of permanent vortex fragments. These multi-scale fragments then separate from the voids and cracks in the microstructure interfaces and boundaries [35] as wear debris, bringing about the consequent fragmentation and delamination of surface materials during the stable wear stage (Fig. 11b). Such phenomenon is assumed to be the main cause for wear

rate increase in slow-to-stable wear transition and the relatively high wear rate in stable wear stage. Therefore, it can be concluded that the cyclic process of spalling and regrowing is the main character of vortex structure evolution during the stable wear stage, while the wear mechanism during this stage manifests itself in the periodic procedure of strain accumulation and plastic failure below the worn surface.

5 Conclusions

Dry sliding wear tests of normalized 40Cr steel were conducted under various sliding distances through disc-on-pin configuration. The dynamic deformation, microstructural evolution beneath worn surface and their effects on the wear behavior of 40Cr pins were systematically investigated. The main research conclusions are as follows:

- (1) Three typical wear stages, which successively corresponded to the initial wear, slow wear and stable wear, could be divided according to the wear rate variations with the prolongation of sliding distances.
- (2) The worn subsurface structures of normalized 40Cr steel involved the unpeeled delamination layer and plastic deformation layer, exhibiting a gradually decreased microhardness distribution varying from over 390 $HV_{0.01}$ of the outmost layer to 200 $HV_{0.01}$ of the matrix.
- (3) Nanocrystalline grains with the size of 40–100 nm were generated in the outmost worn subsurface. The subsurface nanocrystallization during friction could involve four processes: pearlite interlamellar space reducing accompanied with dislocations developing; cementite lamellar fracturing and partly dissolving; the transformation of dislocation walls into low-angle subboundaries, dividing the original grains into more subgrains; the transition from low-angle boundaries into high-angle grain boundaries, refined grains further subdivided until reaching the stable minimum level.
- (4) Severely deformed vortex structures formed in the upmost worn subsurface as a result of high strain localization and shear instability during the slow wear stage,

exhibiting a relatively high microhardness and brittleness. The periodically forming and delaminating process was the main feature of vortex structure evolution, accounting for the wear rate increase in slow-to-stable wear transition. The wear mechanism during stable wear stage manifested itself in the cyclic procedure of strain accumulation and plastic failure below the worn surface.

References

- Moore, M.A., Douthwaite, R.M.: Plastic deformation below worn surfaces. *Metall. Trans. A* **7**(12), 1833–1839 (1976)
- Rainforth, W.M., Stevens, R., Nutting, J.: Deformation structures induced by sliding contact. *Philos. Mag. A* **66**(4), 621–641 (1992)
- Rigney, D.A., Glaeser, W.A.: The significance of near surface microstructure in the wear process. *Wear* **46**(1), 241–250 (1978)
- Markov, D., Kelly, D.: Mechanisms of adhesion-initiated catastrophic wear: pure sliding. *Wear* **239**(2), 189–210 (2000)
- Su, T.F., Han, X., Wang, Y.B., Yin, M.L., Liang, C., An, J.: An investigation on subsurface microstructural evolution and mild to severe wear transition in AZ51 magnesium alloy. *Tribol. Trans.* **58**(3), 549–559 (2015)
- Rigney, D.A., Karthikeyan, S.: The evolution of tribomaterial during sliding: a brief introduction. *Tribol. Lett.* **39**(1), 3–7 (2010)
- Yao, B., Han, Z., Lu, K.: Correlation between wear resistance and subsurface recrystallization structure in copper. *Wear* **294**, 438–445 (2012)
- Korres, S., Feser, T., Dienwiebel, M.: In situ observation of wear particle formation on lubricated sliding surfaces. *Acta Mater.* **60**(1), 420–429 (2012)
- Sun, H.Q., Shi, Y.N., Zhang, M.X.: Sliding wear-induced microstructure evolution of nanocrystalline and coarse-grained AZ91D Mg alloy. *Wear* **266**(7–8), 666–670 (2009)
- Sato, H., Kaneko, Y., Watanabe, Y.: Effects of work hardening rate on formation of nanocrystallized subsurface layer in Cu alloys. *Japanese Journal of Applied Physics* **56**(1S), 01AE05 (2016)
- Liu, X.C., Zhang, H.W., Lu, K.: Strain-induced ultrahard and ultrastable nanolaminated structure in nickel. *Science* **342**(6156), 337–340 (2013)
- Chen, X., Han, Z., Li, X., Lu, K.: Lowering coefficient of friction in Cu alloys with stable gradient nanostructures. *Sci. Adv.* **2**(12), e1601942 (2016)
- Liu, Y., Jin, B., Lu, J.: Mechanical properties and thermal stability of nanocrystallized pure aluminum produced by surface mechanical attrition treatment. *Mater. Sci. Eng. A* **636**, 446–451 (2015)
- Wang, X., Wei, X., Hong, X., Yang, J., Wang, W.: Formation of sliding friction-induced deformation layer with nanocrystalline structure in T10 steel against 20CrMnTi steel. *Appl. Surf. Sci.* **280**, 381–387 (2013)
- Chromik, R.R., Zhang, Y.: Nanomechanical testing of third bodies. *Curr. Opin. Solid State Mater. Sci.* **22**(4), 142–155 (2018)
- Dautzenberg, J.H., Zaat, J.H.: Quantitative determination of deformation by sliding wear. *Wear* **23**(1), 9–19 (1973)
- Kato, H., Sasase, M., Suiya, N.: Friction-induced ultra-fine and nanocrystalline structures on metal surfaces in dry sliding. *Tribol. Int.* **43**(5–6), 925–928 (2010)
- Zhang, Y.S., Zhang, P.X., Niu, H.Z., Chen, C., Wang, G., Xiao, D.H., Bai, X.F.: Surface nanocrystallization of Cu and Ta by sliding friction. *Mater. Sci. Eng. A* **607**, 351–355 (2014)
- Tarasov, S., Rubtsov, V., Kolubaev, A.: Subsurface shear instability and nanostructuring of metals in sliding. *Wear* **268**(1–2), 59–66 (2010)
- Yao, B., Han, Z., Li, Y.S., Tao, N.R., Lu, K.: Dry sliding tribological properties of nanostructured copper subjected to dynamic plastic deformation. *Wear* **271**(9–10), 1609–1616 (2011)
- Wasekar, N.P., Haridoss, P., Seshadri, S.K., Sundararajan, G.: Sliding wear behavior of nanocrystalline nickel coatings: influence of grain size. *Wear* **296**(1–2), 536–546 (2012)
- Venkataraman, B., Sundararajan, G.: The sliding wear behaviour of Al-SiC particulate composites-II. The characterization of subsurface deformation and correlation with wear behaviour. *Acta Mater.* **44**(2), 461–473 (1996)
- Sato, H., Murase, T., Fujii, T., Onaka, S., Watanabe, Y., Kato, M.: Formation of a wear-induced layer with nanocrystalline structure in Al-Al₃Ti functionally graded material. *Acta Mater.* **56**(17), 4549–4558 (2008)
- Cai, W., Bellon, P.: Subsurface microstructure evolution and deformation mechanism of Ag-Cu eutectic alloy after dry sliding wear. *Wear* **303**(1–2), 602–610 (2013)
- Panin, V., Kolubaev, A., Tarasov, S., Popov, V.: Subsurface layer formation during sliding friction. *Wear* **249**(10–11), 860–867 (2001)
- Yin, C.H., Liang, Y.L., Jiang, Y., Yang, M., Long, S.L.: Formation of nano-laminated structures in a dry sliding wear-induced layer under different wear mechanisms of 20CrNi2Mo steel. *Appl. Surf. Sci.* **423**, 305–313 (2017)
- Lojkowski, W., Djahanbakhsh, M., Bürkle, G., Gierlotka, S., Zielinski, W., Fecht, H.J.: Nanostructure formation on the surface of railway tracks. *Mater. Sci. Eng. A* **303**(1–2), 197–208 (2001)
- Zhang, H.W., Ohsaki, S., Mitao, S., Ohnuma, M., Hono, K.: Microstructural investigation of white etching layer on pearlite steel rail. *Mater. Sci. Eng. A* **421**(1–2), 191–199 (2006)
- Xu, Y., Fang, L., Cen, Q., Zhu, J.: Nano structure and transformation mechanism of white layer for AISI1045 steel during impact wear. *Wear* **258**(1–4), 537–544 (2005)
- Zhou, L., Liu, G., Han, Z., Lu, K.: Grain size effect on wear resistance of a nanostructured AISI52100 steel. *Scripta Mater.* **58**(6), 445–448 (2008)
- Pan, R., Ren, R., Chen, C., Zhao, X.: Formation of nanocrystalline structure in pearlitic steels by dry sliding wear. *Mater. Charact.* **132**, 397–404 (2017)
- Tao, N.R., Wang, Z.B., Tong, W.P., Sui, M.L., Lu, J., Lu, K.: An investigation of surface nanocrystallization mechanism in Fe induced by surface mechanical attrition treatment. *Acta Mater.* **50**(18), 4603–4616 (2002)
- Schouwenaars, R., Jacobo, V.H., Ortiz, A.: Microstructural aspects of wear in soft tribological alloys. *Wear* **263**(1–6), 727–735 (2007)
- Psakhie, S.G., Zolnikov, K.P., Dmitriev, A.I., Smolin, A.Y., Shilko, E.V.: Dynamic vortex defects in deformed material. *Phys. Mesomech.* **17**(1), 15–22 (2014)
- Kolubaev, A., Tarasov, S., Sizova, O., Kolubaev, E.: Scale-dependent subsurface deformation of metallic materials in sliding. *Tribol. Int.* **43**(4), 695–699 (2010)

Publisher's Note Springer Nature remains neutral with regard to jurisdictional claims in published maps and institutional affiliations.